frontiers in Materials

ORIGINAL RESEARCH
published: 06 November 2020
doi: 10.3389/fmats.2020.563233

Microstructure and Composition of Red Mud-Fly Ash-Based Geopolymers Incorporating Carbide Slag

Yuxuan Shi[1,2], *Zhaoyun Zhang*[3], *Zhaohu Sang*[3] *and Qingxin Zhao*[1,2]*

[1]State Key Laboratory of Metastable Materials Science and Technology, Yanshan University, Qinhuangdao, China, [2]Key Laboratory of Green Construction and Intelligent Maintenance for Civil Engineering of Hebei Province, Yanshan University, Qinhuangdao, China, [3]Tangshan Sanyou Alkali Chloride Co., Ltd., Tangshan, China

In order to find the possibility of recycling an industry waste solid red mud from earth, a kind of geopolymer material system based on red mud-fly ash-carbide slag has been developed entirely from waste. The microstructure and composition of the geopolymer material system at the age of 28 days was tested by the scanning electron microscope (SEM), back scattered electron (BSE), energy dispersive spectroscopy (EDS), X-ray diffraction (XRD) and thermogravimetric-differential scanning calorimetry (DSC-TG). It was showed that the compressive strength of the geopolymer sample was 15.1 MPa when the liquid solid ratio (L/S) was 0.7, sand-binder ratio was 3:1, alkaline activator used wet-based carbide slag, and the fly ash, red mud and carbide slag were prepared as the proportion of 4:3:3. Through scanning electron microscope, back scattered electron, energy dispersive spectroscopy, X-ray diffraction, and thermogravimetric-differential scanning calorimetry results, the spherical beads in fly ash were dissolved in the alkaline environment to form silicon and aluminum monomers and polymerized to synthesize C-S-H and C-A-S-H gels. Wet-based carbide slag played the role of calcium component support in C-A-S-H, C-S-H gels and alkaline activator.

Keywords: geopolymer, red mud, fly ash, carbide slag, alkali-activated

OPEN ACCESS

Edited by:
Dongshuai Hou,
Qingdao University of Technology, China

Reviewed by:
Xiaojian Gao,
Harbin Institute of Technology, China
Hongxia Qiao,
Lanzhou University of Technology, China

***Correspondence:**
Qingxin Zhao
zhaoqx2002@163.com

Specialty section:
This article was submitted to Structural Materials, a section of the journal Frontiers in Materials

Received: *18 May 2020*
Accepted: *21 August 2020*
Published: *06 November 2020*

Citation:
Shi Y, Zhang Z, Sang Z and Zhao Q (2020) Microstructure and Composition of Red Mud-Fly Ash-Based Geopolymers Incorporating Carbide Slag. Front. Mater. 7:563233. doi: 10.3389/fmats.2020.563233

INTRODUCTION

Portland cement consumes a lot of mineral resources and energy during the production process and also brings dust and noise pollution (Song et al., 2019). To reduce cement consumption, geopolymer has gotten more and more attention internationally (Tan et al., 2019; Koutník et al., 2020). Geopolymer is a kind of amorphous aluminium-oxygen-silicate network material formed by mineral condensation of silica-alumina inorganic materials, which is primarily composed of ionic bond and covalent bond, supplemented by Van der Waals bond. Due to their high mechanical properties and environmental benefit, geopolymer appears as a future prospective construction material and have applications in different areas (Singh and Middendorf, 2020). Many solid wastes are often used to synthesize geopolymer such as fly ash, slag, soda residue, red mud, steel slag, and coal gangue (Nie et al., 2016; Yi et al., 2018; Aparicio et al., 2020; Katpady et al., 2020; Vu et al., 2020). Among the above materials, fly ash is the most popular one due to its easy availability all across the globe. Class F fly ash is one of the main raw materials for the preparation of geopolymer, mainly contains spherical beads, which can form silicon and aluminum monomers under alkaline activators, and then forms a gel network through geopolymerization by sharing oxygen atoms (Vu et al., 2020).

Red mud is a kind of solid wastes with high alkalinity from the alumina factories. In China, the annual amount of red mud produced is over 30 million tons. At present, the comprehensive utilization rate of red mud is only 4%, and the accumulated reserves have reached 350 million tons. With the annual increase of alumina production and the decline of ore grade, the storage of red mud will continue to increase (Hu et al., 2018). The massive storage of red mud has caused serious waste of land resources and severe environmental pollution. Red mud is one of a good substitute for cement, based on its high iron, high silicon, and high aluminum properties. However, compared to the huge output of red mud, the heavy burden of red mud on the environment and society cannot be alleviated by limited utilization. Therefore, more comprehensive utilizations of red mud have been studied by researchers. Zhang et al. (2020) used red mud-derived filler aggregate to replace the limestone powder commonly used in asphalt mastics, and used hydrated lime and white mud to improve red-mud-modified asphalt mastic. When mixed with hydrated lime and white mud, both materials can improve the low temperature crack resistance of red mud asphalt mastic. In addition, the incorporation of the white mud into red mud asphalt mastic can improve its fatigue resistance and moisture resistance of aggregate-mastic bonding under both short- and long-term moisture attack. Zhao et al. (2020) used cement-fly ash-lime to stabilize the sintering red mud, and used the normalized orthogonal table of L9 (34) in the orthogonal test design to obtain the optimal mix ratio of sintering red mud unburned road brick. The compressive strength under standard curing conditions of 28 days was greater than 19 MPa, which has a significant impact on unconfined compressive strength. Geng et al. (2020) proposed an innovative process, co-reduction of municipal solid waste incineration red mud and fly ash followed by magnetic separation, to produce crude alloys and purified slag. Under the best conditions, 92.96% Ni, 85.52% Fe, 80.10% Cu, and 66.74% Cr can be recycled in the Fe-Cu-Ni-Cr alloy. The Fe-Cu-Ni-Cr alloys were composed of 96.47% Fe, 0.81% Cu, 0.65% Ni, and 0.42% Cr can be used to product weathering steel. Removed other metals including Zn, Pb, and Cd by volatilization. Babisk et al. (2019) used plain red mud and incorporations separately to produce bricks and roofing tiles for construction in two different clays, with high-plasticity and low-plasticity clays were for the first time studied. The results showed that according to Brazilian standards, plain red mud can be used as bricks at any of the temperature. When fired at the temperature until 1,050°C, it can be used to produce roof tiles. Alekseev et al. (2019) demonstrated use red mud of hazardous bauxite waste (50–100 wt%), and foundry sand (10–50%) to product new red ceramics composites, replacing the traditional clay-sand mix. The newly developed environmentally friendly ceramics had very high physical properties. The flexural strength value reached 10.54 MPa. Ghalehnovi et al. (2019) determined the fresh and mechanical parameters first, experiments were then conducted in addition to use marble and granite as filler replacement (100%), and different percentages of red mud (2.5%, 5%, 7.5%, and 10%) were used to replace cement production waste. Although the application of red mud has a negative impact on fresh properties, it has been observed that a small amount of red mud mixed with marble and granite has a positive effect on the mechanical behaviors of self-compacting concrete. Cheng et al. (2019) used waste blast furnace slag, red mud and drilling fluid to prepare a new cementitious material. The compressive strength of the samples can reach 16.7 MPa. Microscopic analysis indicated that the new amorphous structure constituted the structure of the hardened paste. The addition of red mud made the structure more dense compared with the blank sample without red mud added. The toxicity leaching result indicated that the heavy metal ion content was within the standard range, proved that the new cementitious material was not harmful to the environment. Singh et al. (2019) recycled polyethylene terephthalate resin (as a binder) artificially mixed with fly ash, red mud and silica fume. Using Taguchi estimates, for the 420-day-cured sample, after increasing the polyethylene terephthalate resin content from 25% to 35%, its compressive strength, indirect tensile strength and bending strength increased by 10.2%, 9.9%, and 11.8%, respectively. The waste material together reduced the water absorption rate. A large number of polyethylene terephthalate resins have increased damping capacity. Silica fume and red mud developed acid resistance.

However, the usage amount of red mud cannot keep up with its production and the needs of the environment and society. In order to make the application range of red mud wider and reduce social pressure, a new type of geopolymer material based on fly ash-red mud-carbide slag has been found. The microstructure and composition were analyzed by SEM, BSE, EDS, XRD and DSC-TG.

EXPERIMENTAL

Raw Materials

The raw materials for this test mainly include red mud, carbide slag, fly ash, and natural river sand. The carbide slag used in the experiment came from San You group in Tangshan, Hebei Province and the red mud came from Xin Fa group in Shandong Province. The red mud was dried naturally and grated to the maximum diameter of 0.16 mm. The XRD pattern of red mud was shown in **Figure 1**. There were no distinct broad humps in red mud, indicated no large quantity of amorphous phases. It was apparent that the phase of Hemmatite, Calcium Iron Oxide, and Lazurite were contained in the XRD diffraction of red mud. The carbide slag should be stirred evenly in the slurry state before preparing test pieces. The presence of $Ca(OH)_2$ was indicated by the XRD pattern of carbide slag shown in **Figure 2**. The XRD pattern of Class FII fly ash used in the experiment was shown in **Figure 3**. It was showed that the peak of Quartz and Mullite appeared in **Figure 3**, which indicated that Quartz and Mullite were contained in the XRD pattern of fly ash. A wide bump existed between 15° and 40° (2θ) could be observed in the fly ash sample, proved that there was a large number of amorphous phase in the fly ash (Nath et al., 2016). The chemical components of fly ash, red mud and carbide slag obtained by XRF were shown in **Table 1**. A laser particle size analyzer BT-9033H (T) was used to measure the particle size distribution of red mud and fly ash, and the results were shown in

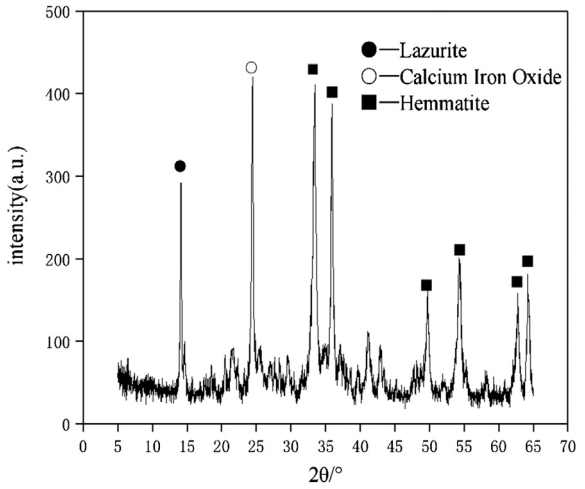

FIGURE1 | XRD diffractogram of red mud.

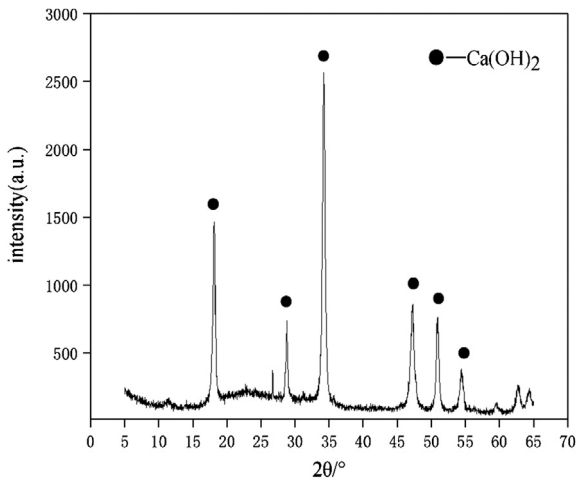

FIGURE2 | XRD diffractogram of carbide slag.

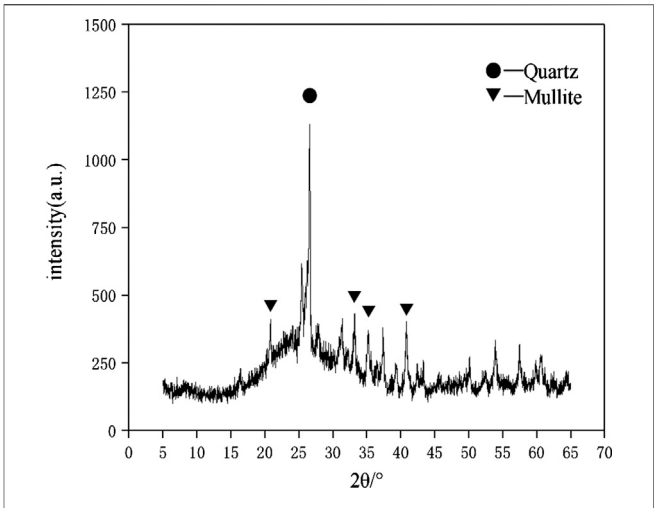

FIGURE 3 | XRD diffractogram of fly ash.

Figure 4. **Table 2** listed other physical properties of red mud and fly ash. Natural river sand had a particle size ranged from 0.16 to 2.36 mm, which granules were well formulated, and the apparent density was 2,750 kg/m^3, the fineness modulus was 2.87 and the mud content was 1.3%.

Preparation of Geopolymers

The carbide slag slurry should be left standing and layered for standby. The upper clear solution was taken out for use as the alkaline activator, which OH ion molarity concentration was 0.052 mol/L, and the pH value was as high as 12.7–12.8. The lower paste had a moisture content of 50%–60% and the effective CaO >80%. The high content of calcium component could improve the overall performance of geopolymers (Temuujin et al., 2009; Huang et al., 2018). In order to reduce the processing procedures, such as grinding and drying, and minimize the utilization cost of industrial solid wastes, the carbide slag was used in a wet-base state during the experimental. And before used the wet-base state of carbide slag, the solid content-density curve must be measured. The measurement data was shown in the **Table 3**. The solid content-density curve of carbide slag was depicted in **Figure 5**. After data fitted, there was a linear relationship between the solid content of wet-based carbide slag (Y_c) and density (ρ) in **Eq. 1**.

$$Y_c = 98.225\,\rho - 84.544 \quad (1)$$

In the mix design of geopolymer samples, the sand-binder ratio was 3:1, the liquid solid ratio (L/S) was fixed at 0.7 and the different percentages of the geopolymer materials were shown in **Table 4**. Solid particles (fly ash, red mud) and wet-based carbide slag were firstly mixed for 3 min, then the upper clear solution of carbide slag was poured into the mixture and evenly stirred for additional 5 min. Thereafter, natural quartz river sand was added and stirred for another 10 min. Then the samples of 40 mm × 40 mm × 160 mm were made successfully. Each mould was vibrated for 2 min on the vibrating table, then covered with a plastic film on the top surface for 24 h. Finally, all geopolymer samples were cured for 7, 14, and 28 days in a box full of water with the temperature was controlled at (20 ± 2)°C, and then were prepared to test compressive strength and flexural strength. Six samples were required for each set of proportions, and the average value was calculated.

Methods

X-Ray Diffraction, Scanning Electron Microscope, and Back Scattered Electron-Energy Dispersive X-Ray Spectroscopy Test of Geopolymers

XRD SEM and BSE-EDS were used to test the factors including microstructure, mineral composition, and gel composition which affects the microscopic characteristics of fly ash-based geopolymers. Followed the test method mentioned in the literature (Aughenbaugh et al., 2016), each set of proportions

TABLE 1 | Chemical composition of fly ash, red mud and carbide slag w/%.

Material	Chemical composition (by mass)/%										
	CaO	SiO_2	Al_2O_3	Fe_2O_3	MgO	TiO_2	P_2O_5	SO_3	MnO	Na_2O	Cl^-
FA	4.67	52.32	32.18	1.58	1.31	—	—	0.56	1.31	—	—
RM	0.95	25.10	32.00	18.90	—	5.28	0.22	0.34	—	16.50	—
CS	87.80	4.71	3.22	0.23	0.39	0.13	0.12	0.78	—	0.43	2.08

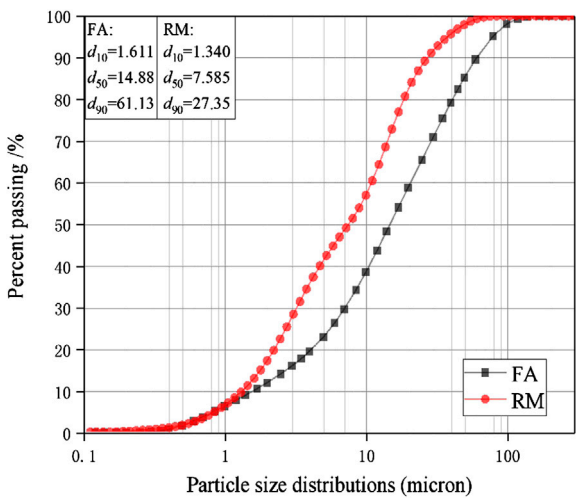

FIGURE 4 | Particle size distributions of red mud and fly ash.

TABLE 2 | Physical properties of red mud and fly ash.

Material	Physical properties	
	Mean particle size, d50 (micron)	Specific surface area/(cm^2/g)
RM	7.585	7,068
FA	14.880	5,036

TABLE 3 | The test data of density and solid content of wet-based carbide slag.

NO.	Density/(g/ml)	Solid quality/g	Liquid quality/g	Solid content/%
1	1.176	47.652	107.637	30.686
2	1.143	43.262	111.494	27.955
3	1.160	45.361	109.455	29.300
4	1.179	42.652	94.493	31.100
5	1.219	44.697	80.856	35.600
6	1.263	45.394	69.819	39.400

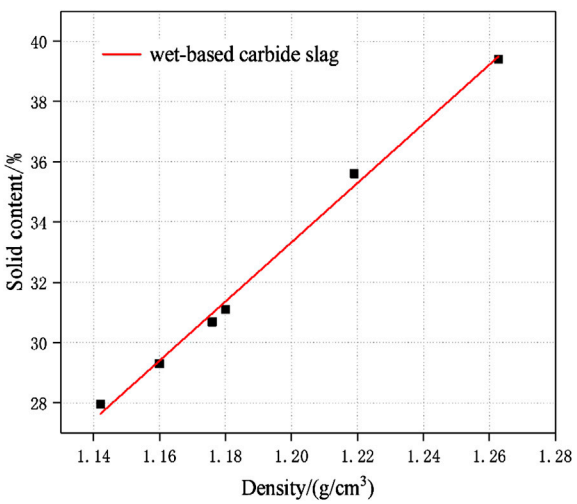

FIGURE 5 | Solid content-density curve of wet-based carbide slag.

in **Table 4** was made into the 20 mm × 20 mm × 80 mm samples, and cured under the same curing conditions. The XRD test samples were taken from the non-carbonized zone in paste sample corresponding to D2. After cured for 28 days, the sample production has the following steps. Firstly, the non-carbonized samples were cut into small slices and put into an isopropanol solution. The isopropanol solution was replaced after 24 h and the immersing was continued for 6 days. Secondly, the samples were taken out from the isopropanol solution and placed in a vacuum dryer for 2–7 days. Then, the samples were ground into powder particles, and about 15 min until the hand felt no graininess. Both insufficient grinding and excessive grinding would cause experimental errors. Finally, put the powder particles in a small vacuum bag to be prepared for XRD test. X-ray diffraction spectroscopy of Rigaku D/MAX-2500/PC with CuK radiation was used with the scanning rate of 2°/min, the voltage of 40 kV, current of 40 mA from 5° to 65° (2θ). The microstructure of the fly ash-red mud based geopolymers at the age of 28 days was tested by the Hitachi-SU8010 SEM. Pieces of paste specimens prepared for SEM test were immersed in isopropanol solution to stop the hydration. Then the small pieces were placed in a vacuum dryer for 2–7 days. At last, the small pieces in a vacuum were taken to the SEM test for photos with different magnifications. The BSE samples need to be flatted and polished in epoxy resin. And the content of the elements of Al, Si, and Ca in the sample was tested by the equipped energy dispersive spectroscopy (EDS).

Thermogravimetric-Differential Scanning Calorimetry Test of Geopolymers

Thermogravimetric differential scanning calorimetry (DSC-TG) was performed on the paste samples at the age of 28 days used the

TABLE 4 | The mix proportion of binders and the strength of the geopolymers samples.

Sample NO.	Mix proportion (by mass)/%			7 days compressivestrength/MPa	7 days flexuralstrength/MPa	28 days compressivestrength/MPa	28 days flexuralstrength/MPa
	Fly ash	Red mud	Carbide slag				
D1	40	40	20	9.50	1.43	11.54	1.58
D2	40	30	30	12.55	1.50	15.10	1.79
D3	40	20	40	10.88	1.47	14.15	1.62
D4	40	10	50	7.63	0.93	10.12	1.25
D5	40	—	60	4.00	0.57	7.03	1.14
D6	50	40	10	7.35	1.12	8.33	1.20
D7	50	30	20	9.72	1.24	11.49	1.48
D8	50	20	30	11.43	1.35	13.92	1.77
D9	50	10	40	8.39	1.12	11.72	1.45

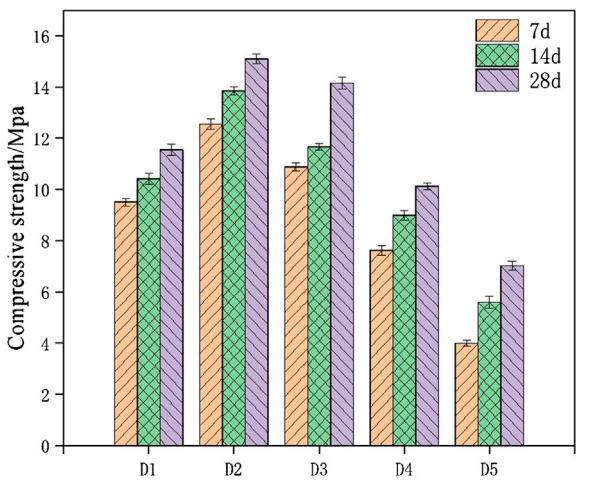

FIGURE 6 | The compressive strength of geopolymers samples.

STA 449F5 integrated thermal analyzer (Zhao et al., 2016). Firstly, the red mud, fly ash and carbide slag were dried in an oven for 12 h, the setting temperature was 105°C, and then the particle size was controlled below 0.9 mm. Secondly, prepared the sample according to the mix proportions in **Table 4**, the liquid solid ratio (L/S) was 0.7. Then put the pastes in a sealed plastic bag and cured in a standard curing cabinet in a controlled environment with the relative humidity ≥95% and (20 ± 2)°C. After cured for 28 days, the fly ash-red mud-carbide slag paste samples should be processed according to the following steps. Firstly, the pastes need be immersed in the isopropanol solution for 7 days and placed in a vacuum dryer for 2–7 days like XRD samples. Secondly, crushed the paste samples into a maximum particle size of 0.12 mm by a standard sieve. And then put the powder sample in the vacuum drying oven for 24 h, the temperature was setted to 105°C. Finally, DSC-TG of the paste specimens at the age of 28 days was performed by the STA 449F5 integrated thermal analyzer. Test parameters were set as follows, the temperature rising rate was 10°C/min, starting temperature 25°C, termination temperature 1,000°C and Ar was used as protective gas to prevent the sample from carbonizing during the heating process.

RESULTS AND DISCUSSION

Mechanical Properties of Geopolymers

Table 4 reveals the compressive strength and flexural strength of geopolymer samples at the age of 7 and 28 days, with different mix proportions. **Table 4** shows that the mechanical characters of D2 group at the age of 28 days was performed the highest value when the fly ash, red mud and carbide slag were prepared as the proportion of 4:3:3. The compressive strength of geopolymers samples cured for 28 days under the ratio of D2 group can reach 15.1 MPa, and the flexural strength of geopolymer samples can reach 1.79 MPa. **Figure 6** shows the compressive strength of geopolymer samples cured for 7, 14 and 28 days with different percentages of raw materials. It can be seen from **Table 4** and **Figure 6** that under the condition that the proportion of fly ash was constant, the compressive strength is positively correlated with the content of red med and negatively correlated with the content of carbide slag. The compressive strength and flexural strength of geopolymer samples under the same condition increase with the curing ages. However, the D5 group has the lowest mechanical strength due to the absence of red mud. For the geopolymer samples of D2 group, the 28 days compressive strength measures 15.1 MPa, which is twice higher than D5 group. It can be seen that the addition of red mud can improve the overall mechanical properties.

Both red mud and carbide slag could provide an alkaline environment to make the amorphous silicate-alumina phases in fly ash dissolved, formed the alumina and silicon monomers. The network aluminosilicate gel was formed by the sharing of oxygen atoms in the polymerization of silicon aluminum monomer (Mehta and Siddique, 2017). The appropriate calcium content in carbide slag could increase the strength of geopolymer by making the fly ash based geopolymers generate C-S-H and C-A-S-H gels (Huseien et al., 2016). Meanwhile, Calcium could accelerate the dissolution of the spherical beads in the fly ash and promote the geopolymerization (Zhao et al., 2019).

Micro-Morphology Analysis of Geopolymers

Paste specimens of geopolymer corresponded to optimal group through the compressive strength and flexural strength test were

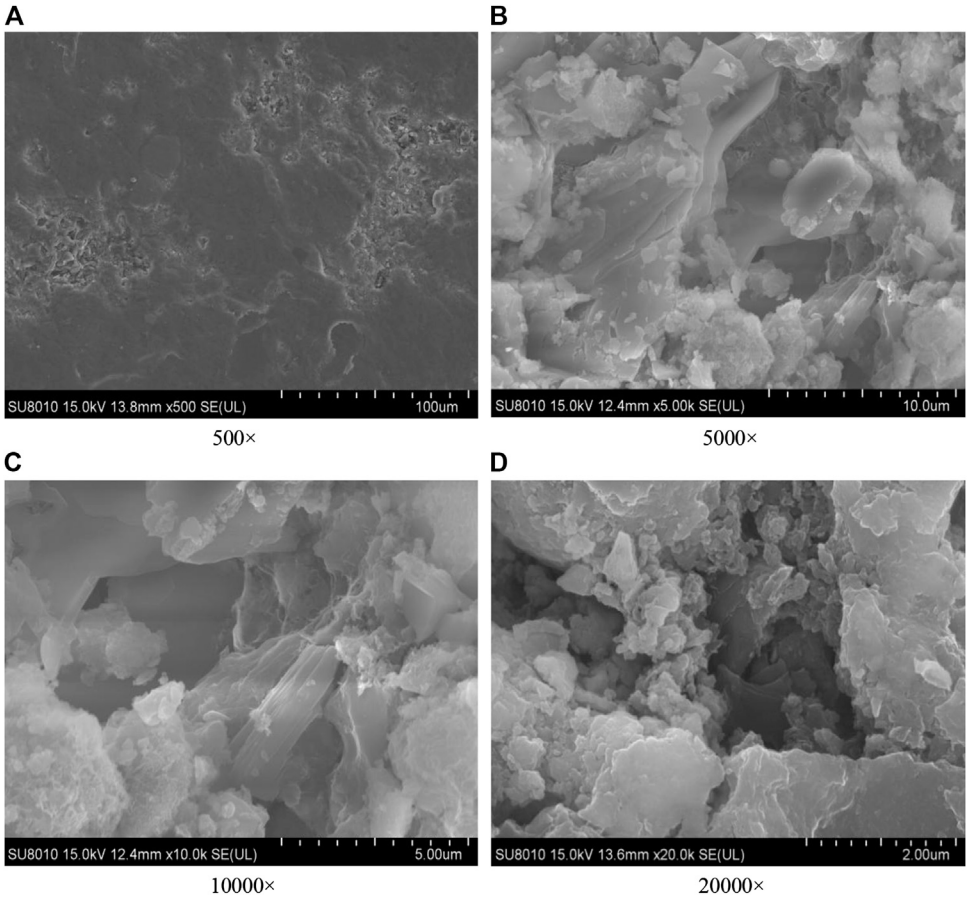

FIGURE 7 | SEM images of the geopolymer specimens of D2 group curing for 28 days.

ready for SEM, which can combine macro strength with micro structure and analyze the composition of amorphous structure. **Figure 7** showed the SEM photographs of geopolymer samples of D2 group at the age of 28 days. The micro structure of the geopolymer samples cured for 28 days begun to form, and the gels structure were dense according to **Figures 7A,B**. The geopolymeric products were abundant, overlap with each other to form a dense three-dimensional network. **Figure 7A** indicated that crystals and gels structure were tightly bounded. The crystals were flaky and layered, and were separated around the amorphous structure. In addition, there was a small amount of unreacted spherical beads around the surface of gels. When the red mud, carbide slag, fly ash and the upper clear solution of carbide slag were mixed, the active Al and Si from fly ash dissolved under alkaline attack and formed the aluminosilicate gels. Although aluminum and silicon accounted for more than half of the red mud composition, a significant portion of them were crystalline and acted as inert filler in the geopolymer binder (Hu et al., 2018). According to the studies, the spherical beads of fly ash was slowly dissolve from the outside to the inside in an alkali-excited environment (Zhao et al., 2019). **Figure 8** shows the dissolved fly ash micro spherical beads. It was indicated that the dissolved fly ash spherical beads were closely bonded with flaky crystals and gels, which could promote further reactions between the active aluminum, silicon monomers in fly ash and with effective calcium components in carbide slag to form C-S-H and C-A-S-H gels, accordingly contributed to a denser structure.

Energy Dispersive Spectrum Analysis of Geopolymers

In order to determine the gel products observed by EDS, relatively uniform sections were found from several micro-regions or spots to obtain chemical element composites and make sure whether other substance existed or not (Zhou and Shen, 2020). BSE samples were taken from the non-carbonized zone of the D2 paste sample of geopolymers. The slices of BSE samples were dipped in an isopropanol solution to stop hydration and then placed in a vacuum dryer for 2–7 days as same as XRD samples. After completing the above steps, the slices of BSE samples were impregnated and polished in epoxy resin to prepare for EDS test. According to research, the atomic number of cnmponents contained in the places and the brightness in the SEM-BSE photos were positively correlated. In SEM-BSE photos, marked the detection points at different brightness positions, and performed EDS analysis for each detection point respectively.

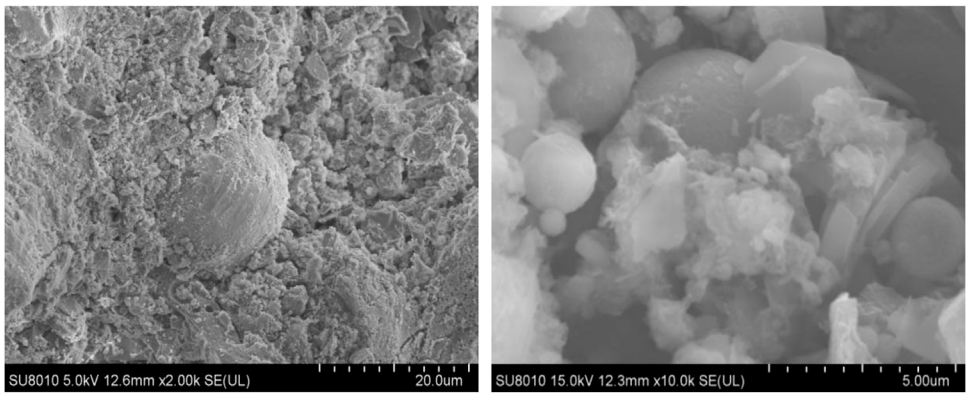

FIGURE 8 | SEM images of dissolved fly ash.

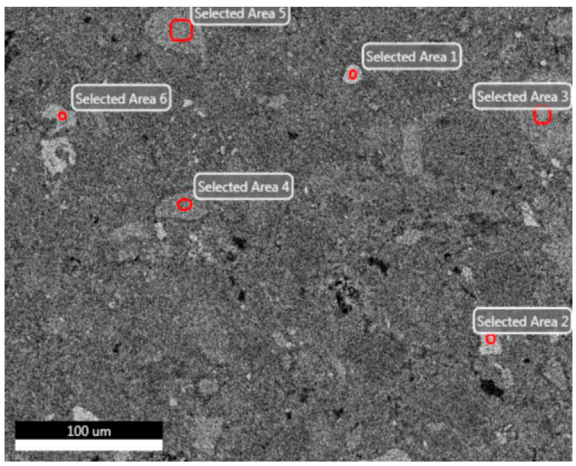

FIGURE 9 | EDS detection dots (300×).

TABLE 5 | Elementary compositions of detection spot.

Location	Elementary compositions (by atomic)/%						
	Si	Al	Fe	Ca	O	Na	Mg
Spot1	1.71	3.28	30.14	1.73	58.89	4.25	—
Spot2	1.98	3.10	29.04	2.00	57.64	5.29	—
Spot3	8.66	5.12	0.48	21.41	61.64	—	—
Spot4	11.15	8.03	—	15.21	55.81	1.49	7.22
Spot5	11.37	7.43	—	15.24	56.82	1.79	6.25
Spot6	1.25	6.85	22.06	2.55	67.10	—	—

The marked positions were seen in **Figure 9**, and the tested results were demonstrated in **Table 5** and **Figure 10**.

It can be seen from the **Figure 9** that the area containing spots 1, 2 and 6 has the highest brightness and the atomic number of components in the SEM-BSE photos. **Table 5** shows that the mass ratio of iron and oxygen elements at spots 1, 2, and 6 was more than 85%, which could prove that the substance in the areas corresponded to three points was the unhydrated red mud particles. . It can be seen from **Figure 9** that the brightness of spots 3, 4, and 5 was almost the same. It was indicated from **Table 5** that the main elements of spots 3, 4, and 5 were Al, Si, O, and Ca. The addition of carbide slag not only provided an alkaline environment, but also supplemented an effective calcium component. The fly ash spherical beads dissolved in an alkaline environment to release monomers of aluminum and silicon which cooperated with the aluminum and silicon elements provided in red mud, the calcium component in carbide slag to form the C-A-S-H and C-S-H gels. Calcium component makes Na_2O-Al_2O_3-SiO_2-H_2O shift to Na_2O-Al_2O_3-SiO_2-CaO-H_2O in fly ash-based geopolymers, which made the formation of different gel products and improved mechanical properties (Garcia-Lodeiro et al., 2011). The extra calcium component could made the fly ash-based geopolymers generate calcium-containing sodium aluminosilicate gel (C, N-A-S-H) or C-S-H and N-A-S-H coexisted, but the most gels were still C-A-S-H and C-S-H (Yip et al., 2007). Therefore, the substance in the areas corresponded to spots 3, 4, and 5 is assumed to be the C-A-S-H and C-S-H gels.

XRD Analysis of Geopolymers

The crystalline state of hydration products affected the mechanical properties and durability directly. The change of the crystal phase can be determined by the XRD spectra. The XRD patterns of geopolymer samples of D2 group at the age of 28 days was shown in the **Figure 11**. The XRD pattern showed a broad and noisy background between 20° and 40° which proved the existence of a large number of amorphous structures in geopolymers (Yang et al., 2019). After geopolymerization, the center of the wide peak moved to a higher angle, which proved the new amorphous have been produced (Bernal et al., 2010). The geopolymer samples of D2 group showed a similar pattern to the sharp peaks in red mud and fly ash. It confirmed that the crystalline phase played the role of inert filling in the three-dimensional network structure (Nie et al., 2016). It was obvious that the mullite phase in the fly ash was gradually disappeared when carbide slag was added, which was indicated that Al_2O_3 participated in the geopolymerization. The original Hemmatite and Lazurite phases in red mud were shown in the XRD pattern, while the Calcium Iron Oxide phase gradually disappeared. This proved that the Calcium Iron Oxide phase in red

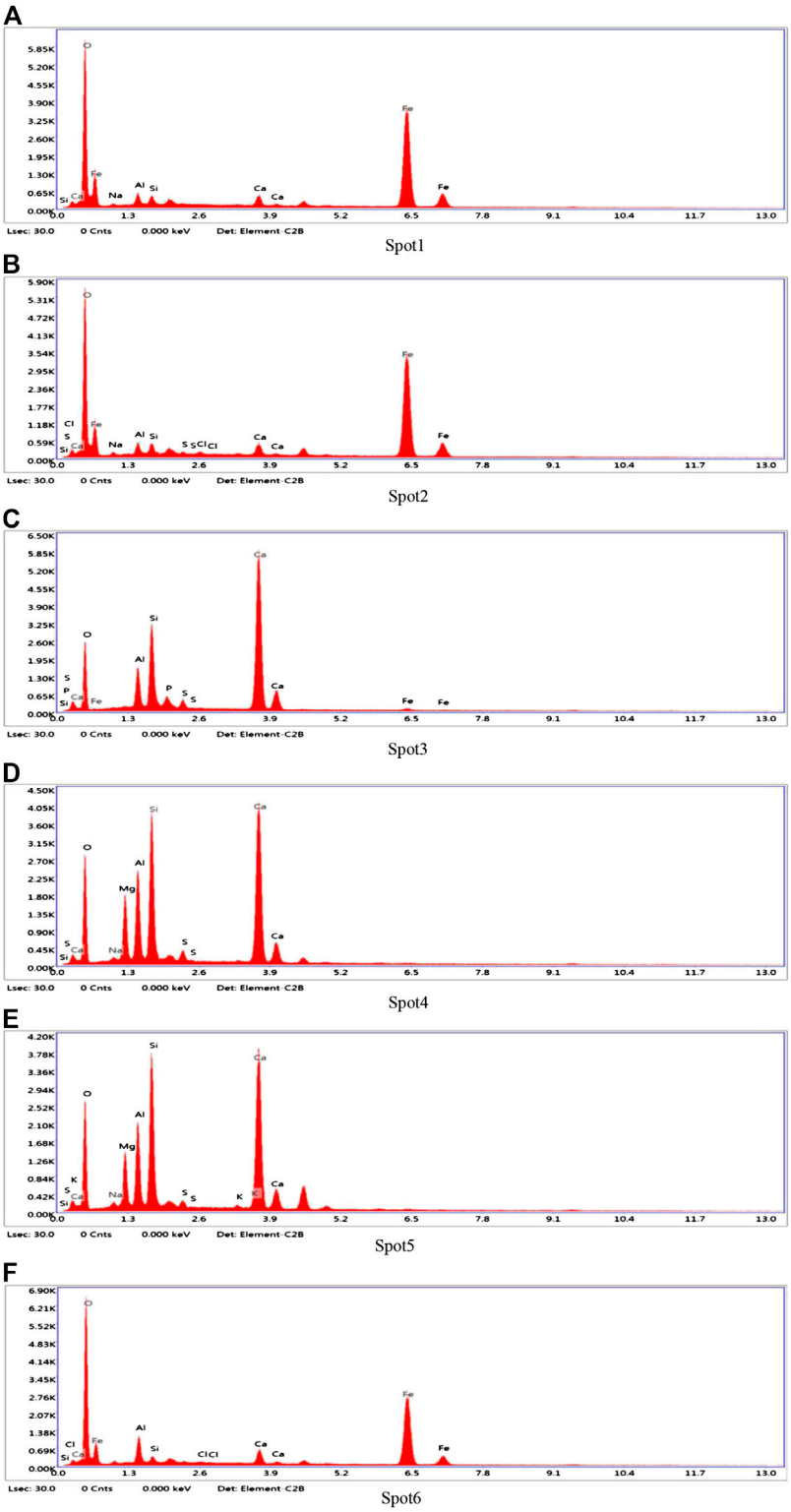

FIGURE 10 | EDS patterns of detection spot.

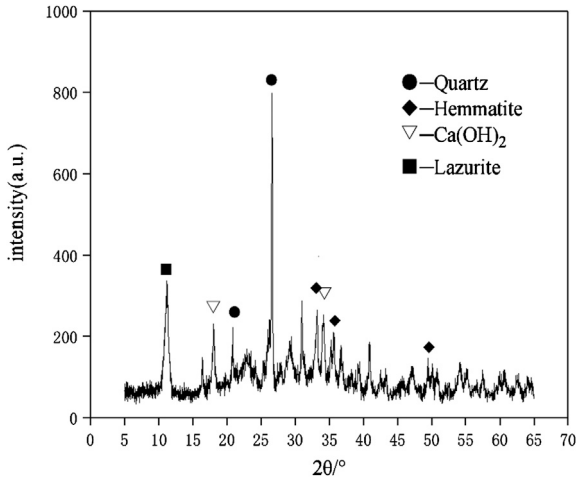

FIGURE 11 | XRD diffractogram of geopolymer specimens of D2 group.

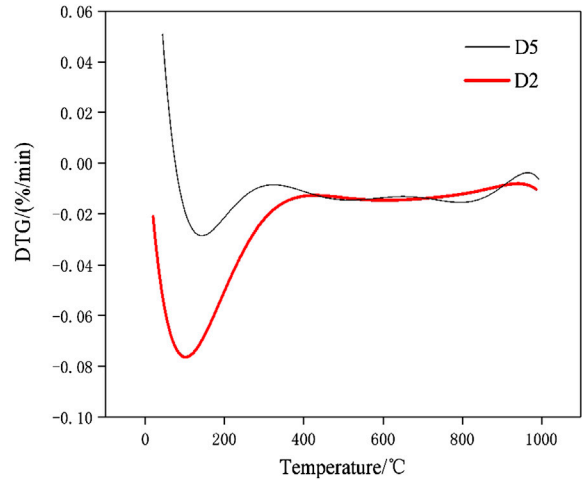

FIGURE 13 | DTG patterns of paste specimens of D2 and D5 groups.

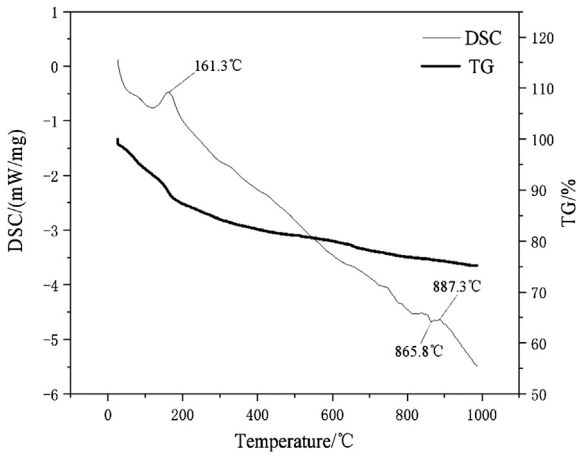

FIGURE 12 | DSC-TG patterns of paste specimens of D2 group.

mud generated C-A-S-H gel and C-S-H gel through geopolymerization. The Hemmatite and Lazurite phases in red mud served as skeleton-filled geopolymer networks. The calcium component was significant for the formation of gel products as a material for C-S-H and C-A-S-H gels. It was showed from **Figure 11** that $Ca(OH)_2$ in carbide slag mostly participated in the geopolymerization.

Thermogravimetric-Differential Scanning Calorimetry Analysis of Geopolymers

The DSC-TG curves of the hydration products of samples D2 at the ages of 28 days were determined in this study and the patterns were shown in **Figure 12**. It can be seen from **Figure 12** that the paste samples of D2 have two main endothermic peaks and two main heat absorption peaks within 1,000°C. The endothermic peaks that located at 161.3°C and 887.3°C respectively. According to the study (Wang and Yan, 2011), the endothermic peak and weightlessness at 161.3°C were due to the loss of free-water and initial decomposition of C-A-S-H gel and C-S-H gel. The sample has only significant weight loss at 161.3°C, indicated that the geopolymer has good thermal stability. The decomposition temperature of carbonate minerals is mostly between 600 and 900°C (Yang and Xue, 2000). For example, dolomite decomposes and releases CO_2 near 800 and 900°C. It can be seen that there was a small endothermic peak at 887.3°C, which was caused by the decomposition reaction of $CaCO_3$ leading to the release of CO_2 and the formation of CaO. The small exothermic peak were at the position of 865.8°C, which was due to the conversion of the crystals of the corresponding C-S-H gel and C-A-S-H gel to β-wollastonite (Wang and Yan, 2008; Liu et al., 2019). After differentiation and fitting, the DTG patterns of paste specimens of D2 and D5 group were shown in **Figure 13**. It can be seen from **Figure 13** that the D2 group with 30% red mud had greater weight loss than the D5 group without red mud. The compressive strengths of the D2 and D5 groups after 28 days of curing were 15.1 and 7.03 MPa. This indicated that the addition of red mud made the geopolymer system synthesis more C-S-H gels and C-A-S-H gels and improve the overall strength. The DSC-TG analysis further confirmed the existence of C-S-H gel and C-A-S-H gel in the hydrated product. In addition to the mass loss of water, both D2 and D5 paste specimens have the similar good thermal stabilities for the microstructure of geopolymers in the range of 25–1,000°C.

Discussion of Results

Portland cement consumes a large amount of mineral resources and energy during the production process, emits a large amount of carbon dioxide, and also brings dust and noise pollution, which do not met the requirements of energy conservation and emission reduction (Habert et al., 2011). In the case of the same output, geopolymers create less than half volume of carbon dioxide compared to Portland cement. In this study, the raw materials of synthetic a new geopolymer were all industrial solid wastes, resulted in a large area of industrial solid wastes were used, which largely replaced Portland cement, protected the

environment and reduced production costs. The high alkalinity of red mud is conducive to promoting the process of geopolymerization and can be consumed in large quantities as a building material.

Many researchers are devoted to the study of using red mud to make fly ash based geopolymers (Yang et al., 2019). And many researches have been devoted to studying different concentrations of NaOH solution, Na_2SiO_3 solution or their mixed solution as alkaline activators to make fly ash geopolymers. According to the study, Huseien et al. (2017) have verified the presence of N-A-S-H gels through microscopic testing methods. Van Riessen et al. (2013) have investigated the use of Bayer process red mud liquid produced by aluminum industry to replace NaOH solution to generate geopolymers. The compressive strength test resulted in the range between 7 and 13 MPa. In this study, the upper clear solution of carbide slag was used instead of the NaOH solution as an alkaline activator, which can save costs better.

Carbide slag and red mud was used to active fly ash in this study, which not only provided an alkaline environment, but also provided effective gel-forming ions. Otherwise, the additional upper clear solution of carbide slag was important to acquire an optimum mechanical character of fly ash based geopolymers. Following the traditionally geopolymerization theory, the geopolymeric three-dimensional network structure are mainly composed of Al, O, Si, and Na. However, the active calcium in carbide slag slag has a positive effect on the mechanical character of the geopolymer, which shows that the final product of this geopolymer cannot be considered as a traditionally geopolymer, but the C-S-H gel and a new geopolymeric structures (Van Deventer et al., 2007). The compressive strength of fly ash based geopolymers with red mud and carbide slag could reach 15.1 MPa in this study. The geopolymers based on red mud, fly ash and carbide slag could meet the minimum strength requirement of the pavement foundation in China (Hu et al., 2018).

CONCLUSIONS

The purpose of this study was to verify the feasibility of preparing fly ash based geopolymers activated by red mud and carbide slag, and to test its crucial performance, including micro-feature and mechanical characteristics. The following conclusions can be drawn.

(1) As the liquid solid ratio (L/S) was 0.7, sand-binder ratio was 3:1, alkaline activator used the upper clear solution of carbide slag, and the fly ash, red mud and carbide slag were prepared as the proportion of 4:3:3, the flexural strength was 1.79 MPa and the compressive strength of the geopolymer sample was 15.1 MPa, which was quite higher to the minimum strength of pavement base and can be used for goaf filling.
(2) Through the microscopic tested results on the geopolymer samples at the age of 28 days, it was indicated that the main geopolymeric products were the C-A-S-H gel and C-S-H gel. Because both red mud and carbide slag could provide an alkaline environment to make the amorphous silicate-alumina phases in the spherical beads in fly ash dissolved, forming the silicon and alumina monomers, which formed gels with calcium in carbide slag through geopolymerization. The crystalline phase acted as an inert filler in the geopolymer network. The gels and the crystalline phase served as skeleton-filled that densely arranged and closely bonded constituted the main strength source of the whole red mud and fly ash based geopolymer system.
(3) Using large industrial solid waste to prepare a new type of geopolymer that can not only solve the problem of solid waste accumulation, but also reduce cement production and pollution. And the use of wet-based carbide slag during the experiment can minimize the utilization cost of industrial solid waste and reduce the treatment process.

DATA AVAILABILITY STATEMENT

The raw data supporting the conclusions of this article will be made available by the authors, without undue reservation.

AUTHOR CONTRIBUTIONS

YS: Experimental design, investigation, methodology and writing. ZZ: Project administration, methodology, investigation and writing. ZS: Supervision, conceptualization, validation, data analysis, and writing. QZ: Funding acquisition, data analysis, methodology and writing.

FUNDING

Financial support from the National Natural Science Foundation of China under the grants of 51578477 and 52078450, the Key R&D Project of Hebei Province under the grant of 19211505D.

REFERENCES

Alekseev, K., Mymrin, V., Avanci, M. A., Klitzke, W., Magalhães, W. L. E., Silva, P. R., et al. (2019). Environmentally clean construction materials from hazardous bauxite waste red mud and spent foundry sand. *J. Constr. Build. Mater.* 229, 116860. doi:10.1016/j.conbuildmat.2019.116860

Aparicio, S., Hernández, M. G., and Anaya, J. J. (2020). Influence of environmental conditions on concrete manufactured with recycled and steel slag aggregates at early ages and long term. *J. Constr. Build. Mater.* 249, 118739. doi:10.1016/j.conbuildmat.2020.118739

Aughenbaugh, K. L., Stutzman, P., and Juenger, M. C. G. (2016). Identifying glass compositions in fly ash. *Front. Mater.* 3, 1–10. doi:10.3389/fmats.2016.00001

Babisk, M. P., Amaral, L. F., Ribeiro, L. D. S., Vieira, C. M. F., Prado, U. S. D., Gadioli, M. C. B., et al. (2019). Evaluation and application of sintered red mud and its incorporated clay ceramics as materials for building construction. *J. Mater. Res. Technol.* 9, 2186–2195. doi:10.1016/j.jmrt.2019.12.049

Bernal, S. A., Gutierrez, R. M. D., Provis, J. L., and Rose, V. (2010). Effect of silicate modulus and metakaolin incorporation on the carbonation of alkali silicate-activated slags. *Cement Concr. Res.* 40, 898–907. doi:10.1016/j.cemconres.2010.02.003

Cheng, X. W., Long, D., Zhang, C., Gao, X. S., Yu, Y. J., Mei, K. Y., et al. (2019). Utilization of red mud, slag and waste drilling fluid for the synthesis of slag-red mud cementitious material. *J. Clean. Prod.* 238, 117902. doi:10.1016/j.jclepro.2019.117902

Garcia-Lodeiro, I., Palomo, A., and Fernandez-Jimenez, D. E. (2011). Macphee, Compatibility studies between N-A-S-H and C-A-S-H gels. Study in the ternary diagram Na2O-CaO-Al2O3-SiO2-H2O. *J. Cem. Conr. Res.* 41, 923–931. doi:10.1016/j.cemconres.2011.05.006

Geng, C., Liu, J. G., Wu, S. C., Jia, Y. F., Du, B., and Yu, S. Y. (2020). Novel method for comprehensive utilization of MSWI fly ash through co-reduction with red mud to prepare crude alloy and cleaned slag. *J. Hazard Mater.* 384, 121315. doi:10.1016/j.jhazmat.2019.121315

Ghalehnovi, M., Roshan, N., Hakak, E., Shamsabadi, E. A., and de Brito, J. (2019). Effect of red mud (bauxite residue) as cement replacement on the properties of self-compacting concrete incorporating various fillers. *J. Clean. Prod.* 240, 118213. doi:10.1016/j.jclepro.2019.118213

Habert, G., Lacaillerie, J. B. D. D., and Roussel, N. (2011). An environmental evaluation of geopolymer based concrete production: reviewing current research trends. *J. Clean. Prod.* 19, 1229–1238. doi:10.1016/j.jclepro.2011.03.012

Hu, W., Nie, Q. K., Huang, B. S., Shu, X., and He, Q. (2018). Mechanical and microstructural characterization of geopolymers derived from red mud and fly ashes. *J. Clean. Prod.* 186, 799–806. doi:10.1016/j.jclepro.2018.03.086

Huang, G. D., Ji, Y. S., Li, J., Hou, Z. H., and Dong, Z. C. (2018). Improving strength of calcinated coal gangue geopolymer mortars via increasing calcium content. *J. Constr. Build. Mater.* 166, 760–768. doi:10.1016/j.conbuildmat.2018.02.005

Huseien, G. F., Mirza, J., Ismail, M., Ghoshal, S. K., and Hussein, A. A. (2017). Geopolymer mortars as sustainable repair material: a comprehensive review. *J. Renew. Sust. Energ. Rev.* 80, 54–74. doi:10.1016/j.rser.2017.05.076

Huseien, G. F., Mirza, J., Ismail, M., and Hussin, M. W. (2016). Influence of different curing temperatures and alkali activators on properties of GBFS geopolymer mortars containing fly ash and palm-oil fuel ash. *J. Constr. Build.* 125, 1229–1240. doi:10.1016/j.conbuildmat.2016.08.153

Katpady, D. N., Takewaka, K., Yamaguchi, T., and Akira, Y. (2020). Performance of slag based Shirasu geopolymer cured under ambient condition. *J. Constr. Build. Mater.* 234, 117210. doi:10.1016/j.conbuildmat.2019.117210

Koutník, P., Soukup, A., Bezucha, P., Šafář, J., and Kohout, J. (2020). Low viscosity metakaolinite based geopolymer binders. *J. Constr. Build. Mater.*. 230, 116978. doi:10.1016/j.conbuildmat.2019.116978

Liu, J. Z., Zhao, Q. X., Zhang, J. R., and An, S. (2019). Microstructure and composition of hardened paste of soda residue-slag complex binding materials. *J. Build. Mater.* 22 (06), 872–877. doi:10.3969/j.issn.1007-9629.2019.06.006

Mehta, A., and Siddique, R. (2017). Sulfuric acid resistance of fly ash based geopolymer concrete. *J. Constr. Build.* 146, 136–143. doi:10.1016/j.conbuildmat.2017.04.077

Nath, S. K., Maitra, S., Mukherjee, S., and Kumar, S. (2016). Microstructural and morphological evolution of fly ash based geopolymers. *J. Constr. Build. Mater.* 111, 758–765. doi:10.1016/j.conbuildmat.2016.02.106

Nie, Q. K., Hu, W., Ai, T., Huang, B. S., Shu, X., and He, Q. (2016). Strength properties of geopolymers derived from original and desulfurized red mud cured at ambient temperature. *J. Constr. Build. Mater.* 125, 905–911. doi:10.1016/j.conbuildmat.2016.08.144

Singh, G., Harmesh Kumar, H., and Sehijpal Singh, S. (2019). Performance evaluation-PET resin composite composed of red mud, fly ash and silica fume. *J. Constr. Build. Mater.* 214, 527–538. doi:10.1016/j.conbuildmat.2019.04.127

Singh, N. B., and Middendorf, B. (2020). Geopolymers as an alternative to Portland cement: an overview. *J. Constr. Build. Mater.* 237, 117455. doi:10.1016/j.conbuildmat.2019.117455

Song, R. J., Zhao, Q. X., Zhang, J. R., and Liu, J. Z. (2019). Microstructure and composition of hardened paste of soda residue-slag-cement binding material system. *J. Front. Mater.* 6, 00211. doi:10.3389/fmats.2019.00211

Tan, J. L., Lu, W. L., Huang, Y. T., Wei, S. J., Xuan, X. X., Liu, L. P., et al. (2019). Preliminary study on compatibility of metakaolin-based geopolymer paste with plant fibers. *J. Constr. Build. Mater.* 225, 772–775. doi:10.1016/j.conbuildmat.2019.07.142

Temuujin, J., Williams, R. P., and Riessen, A. V. (2009). Effect of mechanical activation of fly ash on the properties of geopolymer cured at ambient temperature. *J. Mater. Process. Tech.* 209, 5276–5280. doi:10.1016/j.jmatprotec.2009.03.016

Van Deventer, J. S. J., Provis, J. L., Duxson, P., and Lukey, G. C. (2007). Reaction mechanisms in the geopolymeric conversion of inorganic waste to useful products. *J. Hazard. Mater.* 139, 506–513. doi:10.1016/j.jhazmat.2006.02.044

Van Riessen, A., Jamieson, E., Kealley, C. S., Hart, R. D., and Williams, R. P. (2013). Bayer-geopolymers: an exploration of synergy between the alumina and geopolymer industries. *J. Cem. Concr. Compos.* 41, 29–33. doi:10.1016/j.cemconcomp.2013.04.010

Vu, M. C., Satomi, T., and Takahashi, H. (2020). Influence of initial water, moisture, and geopolymer content on geopolymer modified sludge. *J. Constr. Build. Mater.* 235, 117420. doi:10.1016/j.conbuildmat.2019.117420

Wang, Q., and Yan, P. Y. (2008). Early hydration characteristics and paste structure of complex binding material containing high-volume steel slag. *J. Chin. Ceram.Soc.* 36 (10), 1406–1416. doi:10.14062/j.issn.0454-5648.2008.10.027

Wang, Q., and Yan, P. Y. (2011). The influence of steel slag on the hydration of cement during the hydration process of complex binder. *J. Sci. China Technol. Sci.* 54 (2), 388–394. doi:10.1007/s11431-010-4204-0

Yang, N. R., and Xue, W. H. (2000). *The handbook of inorganic matalloid materials atlas*. Wuhan, China: Wuhan University of Technology Press, 245–267.

Yang, Z. T., Mocadlo, R., Zhao, M. X., Sisson, R. D., Tao, M. J., and Liang, J. Y. (2019). Preparation of a geopolymer from red mud slurry and class F fly ash and its behavior at elevated temperatures. *J. Constr. Build. Mater.* 221, 308–317. doi:10.1016/j.conbuildmat.2019.06.034

Yi, C., Ma, H. Q., Chen, H. Y., Wang, J. X., Shi, J., Li, Z. H., et al. (2018). Preparation and characterization of coal gangue geopolymers. *J. Constr. Build. Mater.* 187, 318–326. doi:10.1016/j.conbuildmat.2018.07.220

Yip, C. K., Lukey, G. C., Provis, J. L., and Van Deventer, J. S. J. (2007). Effect of calcium silicate sources on geopolymerisation. *J. Cem. Concr. Res.* 38, 554–564. doi:10.1016/j.cemconres.2007.11.001

Zhang, J. Z., Li, P. Z., Liang, M., Jiang, H. G., Yao, Z. Y., Zhang, X. M., et al. (2020). Utilization of red mud as an alternative mineral filler in asphalt mastics to replace natural limestone powder. *J. Constr. Build. Mater.* 237, 117821. doi:10.1016/j.conbuildmat.2019.117821

Zhao, Q. X., He, X. J., Zhang, J. R., and Jiang, J. Y. (2016). Long-age wet curing effect on performance of carbonation resistance of fly ash concrete. *J. Constr. Build. Mater.* 127, 577–587. doi:10.1016/j.conbuildmat.2016.10.065

Zhao, X. H., Liu, C. Y., Zuo, L. M., Wang, L., Zhu, Q., and Wang, M. K. (2019). Investigation into the effect of calcium on the existence form of geopolymerized gel product of fly ash based geopolymers. *J. Cem. Concr. Compos.* 103, 279–292. doi:10.1016/j.cemconcomp.2018.11.019

Zhao, Y., Liang, N., Chen, H., and Li, Y. (2020). Preparation and properties of sintering red mud unburned road brick using orthogonal experiments. *Construct. Build. Mater.* 238, 117739. doi:10.1016/j.conbuildmat.2019.117739

Zhou, X. X., and Shen, J. M. (2020). Micromorphology and microstructure of coal fly ash and furnace bottom slag based light-weight geopolymer. *J. Constr. Build. Mater.* 242, 118168. doi:10.1016/j.conbuildmat.2020.118168

Conflict of Interest: Author ZZ and ZS were employed by the company Tangshan Sanyou Alkali Chloride Co. Ltd.

The remaining authors declare that the research was conducted in the absence of any commercial or financial relationships that could be construed as a potential conflict of interest.